Research Square

Preprints are preliminary reports that have not undergone peer review.
They should not be considered conclusive, used to inform clinical practice,
or referenced by the media as validated information.

Cross-reactivity against drifted influenza A (H3N2) subclade K is predicted by pre-existing antibody signatures from recent vaccine targets

Qixin Wang
Harvard T.H. Chan School of Public Health
Lindsay McManus
Harvard T.H. Chan School of Public Health
Daniel Morreale
Harvard T.H. Chan School of Public Health
Samreen Fatima
Harvard T.H. Chan School of Public Health
Ross Blanc
Harvard T.H. Chan School of Public Health
Liping Wang
Beth Israel Deaconess Medical Center
Hadar Malca
Harvard T.H. Chan School of Public Health
Brian Joughin
Massachusetts Institute of Technology
Douglas Lauffenburger
Massachusetts Institute of Technology
Ai-ris Collier
Beth Israel Deaconess Medical Center
Dan Barouch
Beth Israel Deaconess Medical Center
Ryan McNamara
rmcnamara@hsph.harvard.edu

Harvard T.H. Chan School of Public Health

Article

Keywords: Influenza virus, correlates of protection, subclade K, vaccines, systems immunology

Posted Date: November 2nd, 2026

DOI: https://doi.org/10.21203/rs.3.rs-11294133/v1

License: This work is licensed under a Creative Commons Attribution 4.0 International License.
Read Full License

Additional Declarations: Competing interest reported. Q.W. and R.P.M. are co-inventors of SNAb, which is the subject of pending provisional patent applications USSN 63/864,407 and USSN 64/039,079, which are owned by Harvard University. D.H.B. is a co-founder and holds equity in Vector Sciences. Q.W. is currently an employee of CSL Seqirus; Q.W.'s contributions to this work occurred entirely while an employee at the Harvard T.H. Chan School of Public Health. CSL Seqirus played no role in the funding, analysis, or interpretations of this manuscript.

Abstract

Seasonal influenza vaccine strains are selected months before the flu season begins, risking a vaccine mismatch. To that end, quickly predicting protection against newly emerged influenza strains is a public health preparedness need. Further, understanding immunological correlates of protection against mismatched targets is necessary for improving annual influenza vaccination compositions and/or platforms. Using a modified systems-predicted neutralizing antibody (SNAb) approach, we quantified predicted influenza virus neutralization responses in a human cohort pre- and post-vaccination during the 2025/2026 influenza season, during which the vaccine-mismatched H3N2 subclade K accounted for most influenza virus infections. This was done using the previous 10 years of vaccine targets, including the components of the 2025/2026 vaccination, as well as the 2026/2027 vaccine targets. We identified that H3N2 subclade K responders were predicted by baseline SNAb profiles, particularly to the H3N2 components of the 2024/2025 and 2025/2026 influenza vaccine. Systems serological analysis supported this at the multivariate level, with even greater accuracy in predicting mismatched responses from pre-vaccination humoral signatures. Lastly, we employed this approach to predict who would likely be high responders to the 2026/2027 influenza vaccine H1 component, and found that antibody features selected as predicting a strong neutralization response were disproportionately enriched for the H1 component of the 2025/2026 influenza vaccination. Our results support a model in which systems-based approaches can identify signatures predicting strong influenza vaccination responses before the influenza season begins.

Introduction

Seasonal influenza vaccine composition relies on an annual prediction made based on currently circulating and/or emerging strains (1). The strain decision is made ~ 6 months before the flu season starts, which allows for production and distribution of the vaccine. However, newly emergent lineages/subclades of influenza A and influenza B may cause a vaccine mismatch (2). This was the case for the 2025/2026 season.

Influenza A (H3N2) subclade K (J.2.4.1) emerged in 2025 and carried 11 substitutions in hemagglutinin relative to the vaccine strain, 8 of which were located on the hemagglutinin (HA) head, which directly contacts sialic acids for viral entry (3). This subclade rapidly expanded to dominate global H3N2 circulation within a single season (4). A previous study established the neutralization penalty due to antigenic drift in a cohort of influenza-vaccinated participants, with post-vaccination hemagglutinin inhibition (HAI) titers lower for H3N2 subclade K than for direct vaccination targets. This shows at least a partial neutralization escape of this subclade from the vaccine-matched target. However, as a whole, HAI titers did significantly increase from baseline levels against H3N2 subclade K after vaccination (5). To reduce disease burden, subclade K has been included as the H3 component of the 2026 influenza vaccination, replacing the 2025 component H3N2 A/District of Columbia/27/2023.

Few studies have addressed what distinguishes individuals who remain protected against a mismatched strain after influenza virus vaccination. This is largely due to limitations in the quantification of neutralizing antibody titers and the breadth of the readout. Conventionally used methods to estimate influenza virus antibody-based neutralization are microneutralization (MN) and HAI assays, which are inherently limited in dimensionality, such as the number of analytes that can be simultaneously measured (6, 7). There are also differences between HAI and MN assays in terms of mechanism of action (receptor binding inhibition vs. infection inhibition), biologicals used (erythrocytes vs. cultured cells), and titer readouts (endpoint titer vs. 4- parameter fit equation) (8–10). Furthermore, it is not fully understood what antibody features contribute to neutralization of antigenically drifted and vaccine-mismatched influenza virus targets.

We recently developed a systems-predicted neutralizing antibody (SNAb) platform (11), which is a high-throughput, antibody-mediated inhibition assay of a virus receptor binding protein's ability to bind to its cognate receptor. We have adapted this platform to quantify antibody-mediated inhibition of influenza HA binding to α2,6-linked sialic acid in sera. For this study, we have expanded this platform to predict neutralization levels using a Decade of Influenza Virus Antigens (DIVA) panel for the annual influenza vaccine. This DIVA panel includes the 2025 H3 subclade K, as well as targets of the 2026/2027 influenza vaccine composition. We used this panel in parallel with our systems serology platform to interrogate what antibody features were (i) correlated with SNAb titers to the H3 K vaccine-mismatched target, and (ii) predict what antibody features are correlated with the upcoming 2026 H1 vaccine component (A/Missouri/2025 H1N1).

Using serum from vaccinated adult participants, we find that predicted neutralization responses are largely shaped by previous years' influenza vaccine components, even when the circulating strain is mismatched. This was supported both by our high-throughput DIVA panel and by a comprehensive systems serology analysis. We thus propose that systems-based approaches can be utilized to model responses to vaccine-matched and -mismatched targets, and further predict responses based on pre-existing humoral profiles in a high-throughput, volume-sparing, and rapid manner.

Results

SNAb platform profiles the neutralization capacities across a decade of influenza vaccine antigens

To determine what distinguishes individuals who mount protective responses against the drifted, vaccine-mismatched H3N2 subclade K (J.2.4.1) strain during the 2025–26 season, we profiled 42 healthy adults who received the 2025/2026 trivalent inactivated influenza vaccine. Blood draws were collected before (baseline) and three weeks after vaccination (peak) (Fig. 1A, Table 1). Serum was heat-inactivated and processed for serological profiling.

To profile the antibody responses stimulated by influenza virus vaccines, we assembled a Decade of Influenza Virus Antigen (DIVA) panel comprising the hemagglutinin (HA) of 19 influenza A and B strains/targets included in the northern hemisphere seasonal vaccine from 2015/2016 through 2026/2027 (Table 2), together with positive and negative control antigens (**Supplementary Table 1**). Targets from the DIVA panel were assayed in parallel for: (i) systems-predicted neutralizing antibody (SNAb) levels, (ii) antibody isotype (IgG, IgA, IgM) and subclass binding (IgG1, IgG2, IgG3, IgG4, IgA1, IgA2), and (iii) FcγR-binding antibody levels. A downselected group was also assayed for ADNKA responses. Antigens from Influenza B virus (IBV) were included in the isotype, subclass, and FcγR-binding assays. SNAb titers quantified antibody-mediated inhibition of HA binding to α2,6-linked sialic acid and were calculated via 4-parameter fits (4PL) of binding inhibition across serially diluted serum samples. Non-influenza controls such as human serum albumin (HSA) and human cytomegalovirus glycoprotein B (HCMV Gb) were used as specificity controls (**Fig. S1**).

SNAb titers significantly increased from pre- to post-vaccination to all targets within our DIVA panel that passed internal quality control (Fig. 1B, see Methods). SNAb titers to the 2025 K-subclade were modeled through responses to H3N2 A/New York/GKISBBBG87773/2025, which is a research variant validated for serology studies (12). It will be abbreviated as H3N2 A/NY-K/25 for the remainder of this manuscript. Signals against HSA remained at background throughout, confirming that the measured inhibition is influenza HA-specific (Fig. 1B). Baseline median SNAb titers to H3N2 A/NY-K/25 were the lowest of any H3N2 target measured, consistent with other reports (5, 12).

SNAb-inferred HAI titers separate subjects into two populations by inhibitory capacity against H3N2 subclade K at both baseline and peak

The SNAb assay is based on measurement of antibody-mediated inhibition of HA binding to sialic acids, which is shared with the hemagglutinin inhibition assay (HAI). However, SNAb titers are quantified through a 4-parameter logistic regression (4PL), while HAI is usually reported as a discrete endpoint titer. Thus, we assessed how our reported SNAb titers compared with HAI through multiple method comparison analyses. Bland–Altman method agreement analysis showed minimal systematic bias between HAI and SNAb readouts for the H1N1 vaccine component A/Wisconsin/67/2022 (H1N1) (bias 1.10-fold), or the drifted subclade K strain H3N2 A/NY-K/25 (bias 0.71-fold). A Bland-Altman bias score of 0.04 in favor of HAI to A/Wisconsin/67/2022 compared to SNAb was reported, and a bias score of 0.31 in favor of SNAb to H3N2 A/NY-K/25 was reported. All titers were $\log_{10}$-transformed. Thus, the mean reported SNAb titers compared with HAI were within 1.09- and 2.04-fold for H1N1 A/Wisconsin/67/2022 and H3N2 A/NY-K/25, respectively. The majority of paired differences were within ± 0.5 $\log_{10}$ for both targets (**Fig. S2A**). Lin's concordance correlation coefficient (CCC) was 0.781 (95% CI 0.689–0.848) for H1N1 A/Wisconsin/67/2022 and 0.811 (0.733–0.868) for H3N2 A/NY-K/25 (**Fig. S2B**). This would indicate a good-to-excellent assay concordance (13, 14). In both cases, the accuracy component approached unity (0.987 and 0.943), indicating close alignment in location and scale. Precision (Pearson correlation coefficient) was r = 0.79 and r = 0.86, consistent with the Spearman's ρ = 0.76 and ρ = 0.85 (**Fig. S2C**).

We then linked the two assays by Deming regression on $\log_2$-transformed titers, which accounts for measurement error. The fitted equation was $\log_2(\text{SNAb}) = 0.93[95\%\text{CI: } 0.79, 1.06] \times \log_2(\text{HAI}) + 0.91[95\%\text{CI } 0.19, 1.63]$ ($R^2 = 0.739$) (**Fig. S3A**). Inverting this relationship expresses SNAb titers on a continuous inferred HAI scale, on which an HAI titer of 80 corresponds to an SNAb titer of 108, and an HAI titer of 40 equals a SNAb titer of 58.

We quantified responses to H3N2 A/NY-K/25 in our DIVA panel, and if there were any identifiable separations in our cohort of healthy adults to this vaccine-mismatched target using SNAb inferred HAI titers (Fig. 2A). Hartigan's dip test rejected a single-mode (unimodal) distribution in the pooled data ($D = 0.071$, $P = 0.002$) or within each timepoint (peak: $D = 0.089$, $P = 0.009$; baseline: $D = 0.090$, $P = 0.007$). Measuring both single timepoint and pooled collections established that the structure is not an artifact of pooling correlated pre- and post-vaccination samples (Fig. 2B). This also supported that SNAb inferred HAI titers to this vaccine-mismatched target were not normally distributed pre- or post-vaccination. No observations fell between titers of 60.6 and 91.8, and 2 unsupervised criteria were applied to the pooled data to confirm that a logical cut point existed in this titer plateau. The k-means clustering ($k = 2$) and Fisher's 1D discriminant returned the cut points of 65.0 and 74.6, both within the plateau (Fig. 2B). We therefore defined a low-titer population (SNAb inferred HAI ≤ 60.6, total n = 57) and a high-titer population (inferred HAI ≥ 91.8, total n = 27) (Fig. 2C). The two distribution curves interacted at the point which fell into the interval between 60.6 and 91.8. HAI alone did not identify the break within this cohort of low and high titers to H3N2 A/NY-K/25 (**Fig. S3B**). This demonstrates a shortcoming of endpoint analyses for neutralization readouts to influenza and favors a more dynamic quantitation such as a 4PL.

The two populations were not a restatement of vaccination status. Half of the post-vaccination subjects fell into each population (high and low titer), whereas only 6 of 42 subjects were classified as high-titer at pre-vaccination (Fig. 2D). Considered by subject, 21 remained in the low-titer population at both timepoints, 15 converted from low to high following vaccination, and 6 were high titer at both pre- and post-vaccination. This is not to say that participants who remained in the low-titer population had no vaccination response; rather, this response did not move them into the high-titer population. No participant moved from high titer to low titer for H3N2 A/NY-K/25.

Predicted neutralization from recent H3 strains classifies low and high titer groupings against the mismatched subclade K strain.

Having established that subjects separate into two functionally distinct populations by SNAb inferred HAI titers against H3N2 A/NY-K/25, we next sought to investigate any SNAb titers against the strains within our DIVA panel that could separate the low vs. high subclade K SNAb-inferred HAI titer (Fig. 3A). Because none of these individuals had received the drifted subclade K component within the annual influenza vaccination, any signal discriminating against the high- from the low-titer population must derive from cross-reactive responses built against antigenically related strains from current or prior seasons. We initially asked if the high or low H3N2 A/NY-K/25 titers were explained by the most recent

H1 (A/Wisconsin/67/2022 and A/Missouri/11/2025) and H3 (A/District of Columbia/27/2023 and A/Massachusetts/18/2022) cellular/recombinant influenza vaccine targets, both at pre- and post-vaccination **(**Fig. 3B**)**. High H3N2 A/NY-K/25 responders showed pre- and post-vaccination separation from the low titer group for both H3 targets, while only post-vaccination to the H1 targets showed separation between the high and low H3N2 A/NY-K/25 responders. HSA served as a negative control and showed no non-specific binding **(**Fig. 3B**)**.

To more directly test this model, we asked whether the SNAb titer against each DIVA-panel target could classify the populations of low vs. high H3N2 A/NY-K/25 titer at its matched timepoint (Fig. 3A). Each SNAb target was scored by a receiver operating characteristic (ROC) analysis, with an area under the curve (AUC) approaching 1.0 indicating that SNAb titer of the specific target is predictive of the two populations and an AUC near 0.5 indicating no predictive value beyond chance. All the AUC models were cross-validated against the permuted label (random) null models at either timepoint **(Fig. S4)**. Significance was determined for each target by comparing the model AUC with correct low and high H3N2 A/NY-K/25 titer labels to model AUCs generated using permuted labels. Raw SNAb titers, and not SNAb inferred HAI titers, were used for these comparisons.

Among post-vaccination samples, only the most recent H3N2 vaccination targeted strains classified H3N2 A/NY-K/25 population membership with high accuracy (Fig. 3C). H3N2 A/NY-K/25 itself served as the internal positive control (AUC = 1.000 [1.000, 1.000]), followed by H3N2 A/District of Columbia/27/2023, the 2025/2026-season component (AUC = 0.821 [0.789, 0.850]), and H3N2 A/Massachusetts/18/2022, the 2024/2025-season component (AUC = 0.759 [0.723, 0.793]). Assignment between the low and high titer groupings declined sharply with time since the HA was a target of the influenza vaccination. The H3N2 A/Darwin/6/2021 (2023-season component) and other H3 targets from influenza vaccinations of previous years to 2023 fell toward the chance line (AUC ≈ 0.5) in predicting low vs. high H3N2 A/NY-K/25 titers.

The same pattern held when the analysis was performed on pre-vaccination samples (Fig. 3D). H3N2 A/NY-K/25 again separated the populations perfectly (AUC = 1.000 [1.000, 1.000]) as an internal control, while H3N2 A/District of Columbia/27/2023 (AUC = 0.778 [0.729, 0.817]) and H3N2 A/Massachusetts/18/2022 (AUC = 0.862 [0.789, 0.889]) retained strong assignment accuracy, while previous to 2023 H3N2 strains and H1N1 targets remained at or near chance. That the same recent H3N2 strains classify H3N2 A/NY-K/25 population membership (high titer vs. low titer) before and after vaccination supported that responses to this vaccine-mismatched target derived from a pre-existing, cross-reactive antibody pool that vaccination amplifies rather than creates.

H1 responses were also included in this analysis, even though H1-specific antibodies are not expected to cross-react with H3 hemagglutinin. Only post-vaccination H1 targets could predict high vs. low H3N2 A/NY-K/25 titers, which most likely reflects general vaccine responsiveness rather than subtype cross-reactivity, as subjects who present strong responses to one vaccine component tend to respond strongly to all (Fig. 3C, D).

Systems serology profiling can complement predicted neutralizations to identify features contributing to vaccine-mismatched responses

We next used a systems serology approach to interrogate what antibody features may explain high vs. low H3N2 A/NY-K/25 responses. For each of the targets in our DIVA panel, a least absolute shrinkage and selection operator (LASSO)-based partial least squares regression analysis (PLSR) was done, regressing humoral features to the SNAb titer for each target. These LASSO-selected features describing individual SNAb titers would then be used to classify low vs. high H3N2 A/NY-K/25 status, respectively (Fig. 4A). Antibody binding arrays were performed against IAV and IBV HA targets, with consistency and negative response controls (Fig. 4B).

The post-vaccination LASSO-identified signatures correlated with SNAb titers to the vaccine-mismatched H3N2 A/NY-K/25 were used to predict the low vs. high H3N2 A/NY-K/25 titer groups, as a model/approach control **(Fig. S5)**. The LASSO-PLSR identified eight features that defined a minimal set of non-redundant features describing SNAb titer against H3N2 A/NY-K/25. The PLSR model separated subjects along latent variable 1 (LV1), which captured 58.4% of the variance, in a gradient corresponding to measured SNAb titer against H3N2 A/NY-K/25 (**Fig. S5A**). Four features exceeded a variable importance projection score of 1: total IgG, FcγR2A, FcγR2B, and FcγR3A against H3N2 A/NY-K/25 HA (**Fig. S5B**, see Methods). The remaining selected features were IgA1 and IgG2 against H3N2 A/District of Columbia/27/2023, and FcγR3B and IgG2 against H1N1 antigens. The model outperformed both null models (**Fig. S5C**), confirming that the signature reflects information carried by the selected features rather than overfitting. The features with VIP score > 1 correlated strongly with SNAb titer against H3N2 A/NY-K/25 (**Fig. S5D**, top row). Binding features against HSA showed no correlation with the SNAb titer to H3N2 A/NY-K/25, as expected (**Fig. S5D**, bottom row).

Among the post-vaccination dataset, LASSO-PLSR to the two most recent vaccine H3 components (A/District of Columbia/27/2023 and A/Massachusetts/18/2022) showed the highest accuracy in predicting low vs. high H3N2 A/NY-K/25 titers. The LASSO-selected features describing SNAb titers to A/District of Columbia/27/2023 and A/Massachusetts/18/2022 gave predictive AUC = 0.842 [0.783, 0.873] and 0.794 [0.715,0.842] in low vs. high SNAb titers to H3N2 A/NY-K/25, respectively. (Fig. 4C and **Fig. S6**). Similar to our DIVA approach, the LASSO-PLSR showed declining accuracy in predicting low vs. high H3N2 A/NY-K/25 titers with H3 targets pre-2023. Several H1 LASSO-PLSR models showed variable predictive AUC for low vs. high H3N2 A/NY-K/25, with the 2026 component H1N1 A/Missouri/11/2025 showing the highest AUC (Fig. 4C and **Fig. S6**, and **Supplementary Table 2**).

We performed the same analysis at the pre-vaccination collection status to understand if pre-existing immunity could classify low vs. high H3N2 A/NY-K/25 titers. As a model control, post-vaccination LASSO-PLSR of humoral features correlated with SNAb titers to H3N2 A/NY-K/25 was used to predict low vs. high responders to the same strain at the pre-vaccination timepoint. This resulted in a model AUC = 0.968 [0.940–0.991]. We next performed a LASSO-PLSR for post-vaccination H3N2 A/District of

Columbia/27/2023 and H3N2 A/Massachusetts/18/2022 SNAb titers, and asked how the LASSO-selected features could predict low vs. high H3N2 A/NY-K/25 phenotype at the pre-vaccination timepoint. Interestingly, the post-vaccination LASSO features explaining the H3N2 A/District of Columbia/27/2023 titers showed an AUC = 0.948 [0.921–0.972] in correctly identifying low vs. high H3N2 A/NY-K/25 titers. Likewise, the post-vaccination LASSO-PLSR for H3N2 A/Massachusetts/18/2022 SNAb titers showed an AUC = 0.930 [0.894–0.963] in predicting low vs. high H3N2 A/NY-K/25 titers at the pre-vaccination timepoint (Fig. 4D). Thus, a systems serology approach, along with DIVA, supports the model that neutralization against the vaccine-mismatched H3N2 A/NY-K/25 subclade K was likely not created *de novo* by the 2025 influenza vaccine; rather, the features that distinguished high titer individuals were present pre-vaccination, and the 2025 influenza vaccination amplified rather than established them (Fig. 4D and **Fig. S6**).

Signatures derived against three H1N1 antigens: A/Missouri/11/2025, A/Wisconsin/67/2022, and A/Wisconsin/588/2019, also classified H3N2 A/NY-K/25 low vs. high status at post-vaccination (AUC > 0.7, validated against both nulls), but not at pre-vaccination. This was similar to the DIVA results (Fig. 3C, 3D, and 4C, 4D). Thus, predisposition of high titer neutralization to the vaccine-mismatched H3N2 A/NY-K/25 was largely, if not exclusively, through H3 memory. Lastly, there was no concordant effect observed for ADNKA in predicting H3N2 A/NY-K/25 SNAb titers from either H3N2 A/District of Columbia/27/2023, H3N2 A/Massachusetts/18/2022, or H1N1 A/Wisconsin/67/2022 (**Fig. S7**). Likewise, control antigens for non-specific ADNKA showed no distinguishing low vs. high H3N2 A/NY-K/25 titers (**Fig. S8**). These results support that predicted neutralization to the vaccine-mismatched target was strongly correlated with predicted neutralization, binding, and FcγR-binding antibodies at baseline to recent H3 targets of the vaccine, but not with effector functions.

A systems-based approach predicts that high responses to the 2026 H1 influenza component are driven by the 2025 H1 component response

Given that the strongest predictor of high vs. low responses to the vaccine-mismatched H3N2 A/NY-K/25 subclade K was a target of the 2024 influenza vaccine (H3N2 A/Massachusetts/18/2022), we hypothesized that 2025 post-vaccination would predispose a strong response to the 2026 H1 component (A/Missouri/11/2025). In such a model, the post-vaccination collections from the 2025 season would represent the pre-vaccination status of 2026.

To initially test this, correlations between the SNAb titers against H1N1 HA A/Wisconsin/67/2022 and H1N1 HA A/Missouri/11/2025 were calculated pre- and post-vaccination amongst the 2025 cohort. We found that Spearman's ρ between the SNAb titers increased from 0.83 to 0.96 from pre- to post-vaccination collections, respectively, with both Bonferroni-adjusted p-values (q-values) below machine zero (Fig. 5A). Older H1 vaccine targets also showed correlation with H1N1 A/Missouri/11/2025, but to a lesser extent (**Fig. S9**). We next asked what systems serology features were contributing to a LASSO-based PLSR model, regressing to the post-vaccination H1N1 A/Missouri/11/2025 SNAb titers. The LASSO-based PLSR identified FcγR2A H1N1 HA A/Wisconsin/67/2022 as the most significant driver of

the model. Three of the top six LASSO-selected features of the PLSR against H1N1 A/Missouri/11/2025 SNAb titers in the post-vaccination collections were to the 2025 influenza vaccination H1 component A/Wisconsin/67/2022 (Fig. 5B, C).

To validate this approach, the top three selected LASSO features were assessed for correlation with H1N1 A/Missouri/11/2025 SNAb titers from the pre- and post-vaccination collections from the 2025 cohort. Again, the post-vaccination humoral repertoire from this 2025 cohort would establish the foundation for what their 2026 pre-vaccination immune landscape would be. The Spearman's ρ for the top feature, FcγR2A H1N1 HA A/Wisconsin/67/2022, increased from 0.69 to 0.89 in the pre- and post-vaccination collections, respectively (Fig. 5D). The next LASSO-selected feature, IgA1 H1N1 HA A/Wisconsin/588/2019, only showed a statistically significant correlation with SNAb titers to H1N1 HA A/Missouri/11/2025 after vaccination (Fig. 5E); likewise for IgA1 H1N1 HA A/Wisconsin/67/2022 (Fig. 5F).

Collectively, our results support that influenza virus pre-vaccination immune status is a strong predictor of post-vaccination neutralization, both to the direct target of vaccination and to the mismatched H3N2 A/NY-K/25 subclade.

Discussion

Seasonal influenza vaccine strains are selected months ahead of the upcoming flu season, and when the prediction fails and a mismatched strain predominates, the protection effect provided by vaccination relies on cross-reactivity against the mismatched strain. Predictions of cross-reactivity have been difficult to study because it may be reliant on an accumulated exposure history, and no single assay resolves which part of that history is driving the cross-reactive phenotype. Here we applied multiplex neutralization (SNAb) (11) and antibody/Fc-receptor binding (system serology) profiling to identify signatures of cross-reactivity against the vaccine-mismatched H3N2 A/NY-K/25, which accounted for most influenza infections in the 2025/2026 flu season (4, 5). Our approach identified a sharp temporal boundary in the immune history that supports coverage of the drifted strain: antibody signatures explaining HA-binding inhibition of the two most recent H3N2 vaccine antigens classified low vs. high titer with high accuracy, whereas signatures from antigens pre-2023 did not. In other words, the antibody-based neutralization features were likely established before vaccination and were expanded upon by the 2025 vaccination. We cannot discount that infection of a few of the participants occurred between the pre- and post-vaccination collections. Further, we modeled this based on cell and recombinant influenza vaccination composition of the most recent seasons, which may have subtle distinctions from egg-based compositions.

Analysis of the humoral profiles captured in this study revealed that individuals largely fell into two phenotypes against the vaccine-mismatched subclade K H3N2 A/NY-K/25: low titer vs. high titer. This binary response allowed us to utilize a receiver operating characteristic (ROC) to identify whether titers to previous years' influenza vaccination targets could predict whether an individual would be classified

as a low vs. high titer to the H3N2 A/NY-K/25. Moreover, we could perform this operation on pre- and post-vaccination collections to assess if predicted cross-reactivity was a *de novo* process, or a bolstering of an existing one. Our results favor a model in which cross-reactivity to this mismatched target was present at baseline and amplified by vaccination (15–19). The paired structure supports this reading: 6 subjects were already in the high-titer population before vaccination, 15 converted from low to high titers following vaccination, 21 remained in low after vaccination, and none moved from high to low post-vaccination. This is consistent with a model where the seasonal flu shot recalls and expands pre-existing memory shaped by prior exposure, rather than being specifically focused on targets, and it implies that an individual's antibody landscape's capacity to cover a drifted strain may exist and be predicted in a pre-vaccination sample. From a perspective of epidemic preparedness, receipt of the annual flu vaccine would be predicted to broaden against drifted targets.

HAI remains a gold standard in predicting protection against influenza virus strains. A titer of 1:40 is considered protective. This method relies on an endpoint analysis of inhibition of influenza hemagglutinin-dependent erythrocyte agglutination in the presence of antibodies (20–23). We have developed a high-throughput antibody-dependent sialic acid binding inhibition of influenza HA based on a modified approach of mimicking soluble virus receptor binding inhibition. We term this platform SNAb, or a systems-predicted neutralizing antibody assay. This approach uses a 4-parameter logistic regression fit (4PL) model to quantify a serum dilution in which 50% inhibition of HA binding to α2,6-linked sialic acids occurs. As HAI titers are usually quantified through endpoint analysis, we fitted our SNAb titers to HAI levels against the vaccine-mismatched H3N2 A/NY-K/25, resulting in a SNAb inferred HAI titer that was fitted to a 4PL. It was only through this modeling that we were able to identify that individuals fell into two primary phenotypes: low vs. high titer to the vaccine-mismatched H3N2 A/NY-K/25. Beyond the H1 target (A/Wisconsin/67/2022), we could not perform this operation for other influenza vaccination targets (SNAb and HAI titers independently quantified, and then matched across assays), due to limited sample volume, as HAI is not a multiplex-based approach. Statistical assessment of the agreement between SNAb and HAI was strong for both H3N2 A/NY-K/25 and H1N1 A/Wisconsin/2022, consistent with our previous work on SNAb using coronaviruses (11).

The features carrying low vs. high titer assignment information for H3N2 A/NY-K/25 were antigen-specific Total IgG and FcγR binding, and the shared features worked at both pre- and post-vaccination. Other groups and ours have shown that FcγR-binding antibodies are strongly correlated with neutralization readouts (11), and Fc engineering approaches have yielded enhanced or subdued neutralization effects with the same Fab (24, 25). Through a systems serology approach, we identified that FcγR-binding antibodies explaining the most recent two H3N2 vaccine components are a major predictor in the classification of high vs. low titer against H3N2 A/NY-K/25. While FcγR-binding antibodies are linked with effector functions such as ADNKA (26), we did not observe that effector function was a strong predictor in this vaccine-mismatched response. It should be noted that ADNKA to several influenza HA targets, including H3N2 A/NY-K/25, showed high baseline responses, unlike neutralization. Thus, the dynamic range of neutralization and effector function outputs may have skewed our results in favor of the former.

Given that cross-reactivity against H3N2 A/NY-K/25 was largely correlated with responses to previous two years' H3 components of the influenza vaccine, we modeled how the 2025 H1 component would shape profiles to the 2026 H1 influenza vaccine component. The post-2025-vaccination collections would establish their pre-2026-vaccine status, and thus we expected that responses to H1N1 A/Wisconsin/67/2022 would track with H1N1 A/Missouri/11/2025. We found that post-vaccination H1N1 HA A/Wisconsin/67/2022 features, both SNAb titers and system serology-identified features, were strong correlates of SNAb titers to H1N1 A/Missouri/11/2025.

Collectively, our data support the uptake of annual influenza vaccinations, as the immunity built can recognize that year's vaccine targets, as well as establishing baseline immune profiles for subsequent years' strains and/or potential vaccine-mismatched targets. We also propose that pre-vaccination immune profiles are strong predictors of how individuals may have cross-reactivity against emerging strains.

Limitations of the Study

This study has several limitations. (i) The cohort comprises 42 healthy individuals collected at a single site (5). It is not known what factors may have predisposed individuals to higher responses to previous years' H3 components. Higher enrollment studies in distinct geographic regions and with a diversity in age groups would greatly improve our understanding of how pre-existing immunity shapes responses to influenza vaccination. (ii) Our endpoint is a serological titer rather than a clinical outcome, so the framework, at best, predicts a correlate of protection and not protection itself. Also, several participants in the "low titer" group of the H3N2 A/NY-K/25 actually had SNAb inferred titers > 40. Thus, we refrained from calling this "low titer" group non-protected. The cut point between our "low titer" and "high titer" for H3N2 A/NY-K/25 was a SNAb inferred HAI titer of 65 by a K-means cut boundary; this boundary has not been validated as a correlate of protection, and is fit by a 4PL equation and not an endpoint titer. (iii) Not all HA targets could pass internal quality controls for our DIVA panel, and we could not validate each target for SNAb compared with HAI due to sample volume limitations. Our method agreement for H1N1 A/Wisconsin/67/2022 and H3N2 A/NY-K/25 was strong, as well as for other targets previously described (11). That said, direct assay comparison for each target for this cohort would be ideal. (iv) We used our dip analysis of SNAb titers to H3N2 A/NY-K/25 to identify a strong cutoff in titers, and participants largely fell into two groups. However, we did note that there may be hyper-responders in the high titer group, and non-responders in the low titer groups. We were underpowered to further pursue characterizing these phenotypes. (v) As this report was concerned with the vaccine-mismatched H3 K-subclade, and how immune states may predict responses to it and other IAV strains, characterization of antibody profiles generated to IBV was exploratory. Further studies into how neutralization networks are established to IBV and what, if any, impact pre-existing immunity has on IBV vaccination responses is needed.

Methods

Cohort Description

The cohort analyzed in this study is a secondary use from a previous manuscript. Secondary use of the anonymized specimens was approved as not human subjects research by the Harvard IRB (IRB26-0443). Characteristics of the cohort are detailed in Table 1. The original study was conducted at Beth Israel Deaconess Medical Center, and all participants provided informed consent. Assay operators were blinded to infection and vaccination history. Serum samples were separated from peripheral blood draws at the time before vaccination and at peak responses to the vaccination (~ 3 weeks later). Serum was separated from the erythrocytes and leukocytes, and heat-inactivated before use. Aliquots of the heat-inactivated serum were used for the assays to limit freeze-thaw cycles. One sample for each participant at each time collection was used to create the multiple aliquots. Covariates such as age and sex-based influence on the phenotypes were not tested due to enrollment size limitations.

Immunoglobulin Isotyping and Fc-Receptor Binding Affinity Measurement

The measurement of antibody isotype, subclass, and Fc-receptor binding was based on a Luminex multiplexing assay (9, 27–30). Antigens were covalently coupled to carboxylated MagPlex microspheres (Luminex) via NHS-ester linkage using Sulfo-NHS and EDC (Thermo Fisher). The antigen panel comprised influenza hemagglutinin (HA) variants included as seasonal vaccine components from 2015 to 2027, together with SARS-CoV-2 wild-type (WT) and Omicron-lineage (XBB.1.5) spikes as positive controls and human serum albumin (HSA), human coronavirus OC43 (HCoV-OC43) spike, human cytomegalovirus glycoprotein b (HCMV Gb), and Ebola virus glycoprotein (Ebola GP) as negative controls. Heat-inactivated serum samples were then diluted in PBS at 1:500 for IgG2, IgG3, IgG4, IgA1, IgA2, and IgM; 1:2000 for Total IgG, IgG1, and all FcγRs. Diluted sera were incubated with antigen-coupled microspheres for 16 hours at 4°C with constant shaking at 800 rpm to form immune complexes. After incubation, the plates were washed with assay buffer (0.1% BSA and 0.02% Tween-20 in PBS) 3 times and incubated with either PE-coupled secondary antibody (ex., anti-human IgG1-PE) to detect antibody isotypes and subclasses, or PE-labeled FcγR (Duke Human Vaccine Institute) to test for FcγR binding affinity, for 1 hour at room temperature with shaking at 800 rpm. The FcγR was biotinylated first via the BirA500 kit (Avidity) per the manufacturer's instructions. The streptavidin-PE was incubated with the biotinylated FcγR to generate the PE-labeled FcγR. After incubation of all the detectors, the plates were washed 3 times with assay buffer. A total of 40 µL of Luminex Sheath was added to each well, and the plates were then analyzed on the Luminex xMAP INTELLIFLEX® System. All the samples were performed in technical replicates, and the beads only group was treated as a background control for non-specific binding normalization. The reagents and materials used are listed in **Supplementary Table 1**. All binding units were reported as median fluorescence intensity (MFI) in arbitrary units (AU).

Systems-predicted Neutralizing Antibody (SNAb) titer measurements

Receptor-binding specificity was determined via a customized multiplexing system utilizing the same microspheres used in the antibody and FcγR binding assay described above. The HA-coupled microspheres were first incubated with serially diluted serum samples for 16 hours at 4°C with constant shaking at 800 rpm. This step allowed antibodies to bind to regions of the immobilized HA molecules. The plates were washed with assay buffer 3 times and incubated with PE-labeled α2,6-linked sialic acid receptors for 1 hour at room temperature with shaking at 800 rpm. A no-serum control was used to mimic uninhibited binding of HA to PE-labeled α-2,6-linked sialic acid receptors (Top Limit); likewise, a non-α2,6-linked sialic acid-PE detector was used to mimic completely inhibited binding (Baseline). These controls were used for each HA analyte. The plates were washed three times as above. The MFI were captured via the Luminex xMAP INTELLIFLEX® System (**Fig. S1A**). All the samples were performed in technical replicates.

The SNAb titers were calculated based on a 4-parameter (4PL) logistic regression equation fit. If the fitted equation did not achieve an R^2 value > 0.75, the SNAb titer was reported as N/A. Each sample was then quantified for the dilution at which 50% binding inhibition to the HA occurred (SNAb titer) using the fitted curve. The binding inhibition was calculated as follows:

$$Binding\ inhibition\ \% = 100\% \times\ (1 - \frac{Binding_{MFI} - Baseline_{MFI}}{Top\ limit_{MFI} - Baseline_{MFI}})$$

The Top $Limit_{MFI}$ was defined as the mean signal from the positive controls minus 1 standard deviation. Any detected signal ($Binding_{MFI}$) above this limit was normalized to the Top $Limit_{MFI}$. The $Baseline_{MFI}$ was the mean of the negative controls. Binding inhibition exceeding 100% was normalized to 100% (**Fig. S1B**). The reciprocal serum dilution at which binding inhibition was at 50% was used as a reported SNAb titer (11). The reagents and materials used are listed in **Supplementary Table 1**.

Virus neutralization analyses

The HAI results in this manuscript are detailed in their original publication (5).

Antibody-dependent natural killer cell activation (ADNKA)

The HA and Ebola GP antigens (3 μg/mL) were coated onto an ELISA plate for 2 hours at 37°C and then washed with 1X PBS 3 times. The coated plates were then blocked with 5% bovine serum albumin (BSA) diluted in 1X PBS for 1 hour at room temperature. The blocked plates were washed 3 times in 1X PBS, and serum samples were incubated at a 1:25 dilution to form immunocomplexes at 4°C overnight. The Natural Killer (NK) cells were isolated from donor-anonymized Leukopaks (StemCell Technologies) using the EasySep Human NK Cell Isolation Kit (StemCell Technologies). The use of donor-anonymous human luekopaks for ADNKA has been determined as not human subjects research by the Harvard IRB (IRB25-

0685). The isolated NK cells were incubated overnight at 37°C, 5% CO_2, in RPMI-1640 medium (Sigma Aldrich) with 10% fetal bovine serum (FBS) (Sigma Aldrich), 5% penicillin/streptomycin (Corning, 50 µg/mL), 5% L-glutamine (Corning, 4 mM), and 5% HEPES buffer (pH 7.2) (Corning, 50 mM). To the medium, IL-15 at 1ng/mL (StemCell Technologies) was added for activation of the NK cells. After overnight incubation of serum and antigens, the ELISA plates were washed with 1X PBS (3 times), and NK cells (6x10^4/well) were added, along with anti-CD107a–phycoerythrin (PE)–Cy5 (BD Biosciences), brefeldin A (5 µg/mL) (Sigma-Aldrich), and GolgiStop (BD Biosciences). Plates were returned to the 37°C, 5% CO_2 incubator for 5 hours. After the incubation, the NK cells were washed with 1X PBS and stained for surface markers using anti-CD3 Pacific Blue (BD Biosciences), anti-CD16 allophycocyanin (APC)-Cy5 (BD Biosciences), and anti-CD56 PE-Cy7 (BD Biosciences) for 20 minutes at room temperature. Plates were covered with aluminum foil to protect from light. Then the cells were washed and fixed with PermA (Life Technologies) for 15 minutes, and permeabilized with PermB (Life Technologies) and stained for intracellular markers with anti-MIP-1β PE (BD Biosciences) and anti-IFN-γ FITC for 20 minutes at room temperature, protected from light. Then the cells were washed, and the fluorescent intensity was measured using the iQue 3 Cytometer (Intellicyt/Sartorius). NK cells were gated as $CD3^-/CD56^+/CD16^-$. NK activation was evaluated as the positivity percentage of CD107a, IFN-γ, or MIP-1β within the population of $CD3^-/CD56^+/CD16^-$ NK cells. The gating strategy is shown in **Fig. S1C**. All assays were performed with at least two healthy donors, one male and one female. All reagents and materials used are listed in the key resource table. Wells with no serum (PBS-only) on the ELISA plate were used as a negative control for cells to quantify the Lower Limit of Detection (LLOD). Ebola GP was used as an antigen negative control for normalizing non-specific ADNKA.

Computational and Statistical Analysis

Bland-Altman Analyses

Bland–Altman analysis was applied to evaluate method agreement between SNAb and HAI with respect to titer consistency and performance alignment, as described previously (13, 31). Titers from both assays were $\log_{10}$ transformed prior to analysis. For each individual, the mean of the paired HAI and SNAb titers was plotted on the x-axis and the numerical difference between the two assays on the y-axis. This representation allows the discrepancy between assays to be examined across the full range of measured titers rather than at a single point. A mean difference of zero indicates complete agreement (blue dashed line); a positive value indicates bias toward HAI, and a negative value indicates bias toward SNAb. Limits of agreement were defined as the mean difference ± 1.96 standard deviations of the differences (red dashed lines), within which 95% of paired differences are expected to fall.

Lin’s Concordance Correlation Coefficient analysis

Lin’s concordance correlation coefficient (CCC) was used to quantify agreement between SNAb and HAI, complementing the Bland–Altman analysis by resolving agreement into its precision and accuracy components (32). Titers from both assays were $\log_{10}$ transformed prior to analysis. Precision was

calculated as the Pearson correlation coefficient, representing the scatter of the paired observations about the fitted line, and accuracy as the bias correction factor Cb, representing the displacement of that fitted line from the line of perfect agreement. The CCC = precision x accuracy, which penalizes both scatter and systematic bias. Strength of agreement was interpreted using thresholds appropriate to serological method comparison, in which biological and methodological differences between assays impose an inherent ceiling on achievable concordance: poor (CCC < 0.2), fair (0.2–0.4), moderate (0.40–0.60), strong (0.60–0.8), and excellent (≥ 0.8) (10).

Deming Regression fitting

The quantitative relationship between SNAb and HAI was established by Deming regression on $\log_2$-transformed titers, following the approach applied previously to the comparison of hemagglutination inhibition and microneutralization titers for seasonal influenza strains (10, 13, 33). Deming regression rather than linear regression was used to build the conversion between SNAb and HAI titers due to the natural variation caused by the biological assay (four-parameter fit vs. endpoint titer for SNAb and HAI, respectively). Slopes and intercepts were reported with 95% confidence intervals, and a slope whose confidence interval includes unity was taken to indicate proportional agreement between assays. The final equation was reported as: $\log_2(\text{SNAb}) = \text{Slope} \times \log_2(\text{HAI}) + \text{Intercept}$, with R^2 to confirm the significance. This fitted relationship was inverted to express SNAb titers on an inferred HAI scale, and the inferred titer was used for all subsequent classification analyses. All the data points that were quantifiable for SNAb titers were used for building Deming regression fitting for H3N2 A/New York/GKISBBBG87773/2025 (H3N2 A/NY-K/25).

For influenza virus HA SNAb targets that did not have a corresponding HAI titer value, the raw SNAb titers were used as the titer.

Multimodality determination of SNAb-inferred HAI titers

The distribution of SNAb-inferred HAI titers against H3N2 A/NY-K/25 was assessed for multimodality using Hartigan's dip test (34). The dip statistic (D-value, D) and significance (p-value, p) quantify the maximum vertical distance between the empirical cumulative distribution of the data and the closest unimodal distribution, due to the inability to obtain a plateau in a unimodal cumulative distribution, whereas a multimodal cumulative distribution has multiple plateaus. The data cumulative proportion was plotted (y-axis) against $\log_2$-transformed SNAb-inferred HAI titers (x-axis) separately by pooled data, peak dataset, and baseline dataset. D-value (D) and p-value (p) were calculated via dip.test function from the R library "diptest". A D-value > 0.04 with p-value < 0.01 was considered the boundary to determine the multimodality of SNAb-inferred HAI titers. Testing within timepoints was performed because baseline and peak samples from the same subject may be correlated, and thus an oversampling can occur. Individual timepoints are shown to confirm multimodality, and not an artifact of pooling non-independent observations.

The threshold separating the titer populations was determined without supervision. No observation fell between inferred titers of 60.6 and 91.8, a 1.52-fold unpopulated interval. In the pooled data, k-means clustering (k = 2) and Fisher's one-dimensional (Fisher's 1D) discriminant criterion returned cut points for confirming the datapoint separation. The k-means was fitted with 50 random starts, and the boundary was taken as the midpoint between cluster centers. Fisher's 1D criterion was evaluated by exhaustive search over all midpoints to find the most separated split point. Separation between the two populations was quantified by Ashman's D (Ashman's D = 3.60; values > 2 indicate multimodal distribution) and the multimodality index (BI) (BI = 1.59; values > 1.1 indicate multimodality) (35), calculated from component parameters estimated by direct assignment to the two populations. The separation of low vs. high titer was defined as the low titer population as SNAb-inferred HAI titer ≤ 60.6, and the high titer population as SNAb-inferred HAI titer ≥ 91.8.

The distribution of SNAb-inferred HAI titers was displayed as a histogram of $\log_2$-transformed titers with a fixed bin width equal to 1/20 of the observed $\log_2$ titer range. Bars were colored by mixture-assigned population (low vs. high titer or dataset baseline vs. peak). The fitted component densities and their sum (the mixture density) were scaled onto the count axis by multiplying each density by the sample size times the bin width, and a secondary axis reports the corresponding probability density.

SNAb titer based ROC prediction

Each SNAb titer against the flu strains from the DIVA panel at either timepoint was applied individually to perform a receiver operating characteristic (ROC) curve to identify the binary classifier of low vs. high SNAb-inferred HAI titer against H3N2 A/NY-K/25. The binarized classifier of low vs. high SNAb titer was decided by analysis, k-means clustering, and Fisher's 1D discrimination listed above.

Models were fitted independently either on the $\log_{10}$-transformed peak or the $\log_{10}$-transformed baseline dataset, and the classification performance was assessed by 100 cross-validation repetitions, with a total of 100 permuted label (random) null models separately. Areas under the curve (AUC) are reported with bootstrap 95% confidence intervals, and the lower limit of predictive ability (LLPA) for classification is AUC = 0.5, which means a 50% chance of correct prediction. The model built on H3N2 A/NY-K/25 SNAb titers to classify the high and low NY-K titer population is reported as an internal positive control at either timepoint, considering that both classification and prediction were done by the same numeric variable under the same dataset. The p-value to report the significance between the true model and null model was assessed by empirical permutation testing, and $p < 0.05$ was considered a validated prediction.

LASSO-PLSR

Total antibody outputs and SNAb titers were $\log_{10}$ transformed and z-scaled, and the antibody binding levels were background-subtracted before multivariate analysis: supervised clustering through a partial least squares regression (PLSR). Before PLSR modeling, a least absolute shrinkage and selection operator (LASSO) ($\alpha = 1$) was employed to identify a minimal set of non-redundant features that could

describe the continuous numeric variables of SNAb titers against each antigen in the DIVA panel at the multivariate level at the peak dataset. Within each LASSO trial, the regularization penalty (λ) was selected by 5-fold cross-validation, four folds were used for fitting and the fifth for evaluation. This process was repeated 5 times, as each fold was withheld once to identify the best performing λ, which was then used to fit the final LASSO model. The LASSO trial was repeated 100 times, with features selected by at least 75% of all models. If no feature met this criterion, the most frequently selected feature was retained as the only feature, which also means no model could be built. The retained features were used to train a PLSR model with two latent variables (LV1 and LV2). To test the accuracy of the model, a parallel operation was performed with the same parameters (α = 1, folds = 5, threshold = 75%) to test the coefficient of determination (R^2) from the trained model (4/5 folds of data) on the tested model (1/5 fold of data). The R^2 was generated 5 times with each fold withheld once, and the averaged R^2 will be used as the reported one. To determine the model performance, the cross-validation was repeated 50 times, and each time of cross-validation with 50 times of two null models: the random-feature model, in which an equal number of features were drawn at random from the full feature space, and the permuted-label model, in which the outcome values were randomly reassigned across subjects. The random-feature null hypothesis establishes that the selected features carry information beyond that available from arbitrary measurements, and the permuted-label null hypothesis establishes that the model is not fitting noise. Each null model was repeated 50 times per cross-validation trial, yielding 2500 null models of each type per target. Model validation was performed via cross-validated R^2 (R^2Y), computed from out-of-fold predictions of individual SNAb titers pooled across all folds and evaluated over repeated 5-fold cross-validation runs, and the same principle was used in null-model validation.

The list of features for explaining the SNAb titers was considered validated when it met two criteria together: 1. the R^2 of the true model showed a significant difference compared to either null model; 2. $R^2 > 0$. The lower limit of predictive ability (LLPA) was defined as $R^2 = 0$. The p-value to assess the significance between the true model and the null model was assessed by empirical permutation testing.

Regression based LASSO-feature selection for ROC prediction

Signatures identified against each SNAb target in the peak dataset were carried forward to test whether the same antibody features distinguish individuals reaching a high inferred titer against the mismatched subclade K strain. The feature list was generated from the peak-derived antibody features from LASSO selection against individual SNAb titers against the HA targets in the DIVA panel. After selecting the features, the features were applied to perform a receiver operating characteristic (ROC) curve to identify the binary classifier of low vs. high SNAb-inferred HAI titer against H3N2 A/NY-K/25, decided dip analysis, k-means clustering, and Fisher's 1D discrimination listed above.

Models were fitted independently within the peak dataset and within the baseline dataset, and the classification performance was assessed by 100 cross-validation repetitions, with a total of 100 permuted label (random) null models, at each timepoint separately. Areas under the curve (AUC) are

reported with bootstrap 95% confidence intervals, and the LLPA for classification is AUC = 0.5, which means the prediction is at a 50% chance. The model built on anti- H3N2 A/NY-K/25 features to classify H3N2 A/NY-K/25 functional status at the peak dataset is reported as an internal positive control, considering that both classification and LASSO-PLSR were done by the same numeric variable under the same dataset. The p-value to represent the significance between the true model and null model was assessed by empirical permutation testing. Considering the AUC were generated from both LASSO-PLSR and ROC curves, they must meet all the criteria: (i) $p < 0.05$ from both LASSO-PLSR and ROC; (ii) at least an $R^2 > 0$; and (iii) at least an AUC > 0.5 to consider a valid prediction.

A LASSO-based PLSR was performed to identify features correlating with H1N1 A/Missouri/11/2025 post-vaccination. Given that the distribution profile of SNAb titers did not form a binary outcome, direct pre- and post-vaccination correlations of the LASSO-identified features were done instead of an ROC analysis.

Univariate analysis

Univariate comparisons of antibody features and ADNKA between subjects above and below the SNAb inferred HAI threshold were performed separately at baseline and at peak. Because feature distributions are non-normal and sample sizes are unequal between groups, comparisons used the two-sided Wilcoxon test. Correction for multiple comparisons across features was applied by the Benjamini–Hochberg procedure. Significance is indicated as * $p < 0.05$, ** $p < 0.01$, *** $p < 0.001$; ns, not significant. Correlations between different SNAb titers and individual antibody features were assessed by Spearman rank correlation on log-transformed values, with correlation coefficients reported as a Spearman's rho (ρ) and Bonferroni-adjusted p-values as q-values. Non-specific control antigens, including human serum albumin and Ebola virus glycoprotein, were analyzed identically and are reported alongside the specific antigens to demonstrate that the observed associations do not reflect non-specific binding.

Declarations

Acknowledgements

The authors would like to thank the anonymized participants in this study. This work was funded by Harvard University William F. Milton Fund (A.Y.C.), Massachusetts Consortium for Pathogen Readiness (A.Y.C.), National Institutes of Health Grant CA260476 (D.H.B.), National Institutes of Health Grant P01AI165072 (R.P.M.), National Institutes of Health Grant U19AI135995 (D.A.L. and R.P.M.), and National Institutes of Health Contract 75N93021C00029 (R.P.M.).

Declarations of Interest

Q.W. and R.P.M. are co-inventors of SNAb, which is the subject of pending provisional patent applications USSN 63/864,407 and USSN 64/039,079, which are owned by Harvard University. D.H.B. is a co-founder and holds equity in Vector Sciences. Q.W. is currently an employee of CSL Seqirus; Q.W.'s contributions

to this work occurred entirely while an employee at the Harvard T.H. Chan School of Public Health. CSL Seqirus played no role in the funding, analysis, or interpretations of this manuscript.

Data Availability Statement

Raw data used for this manuscript is deposited on the HSPH Systems Serology GitHub page under the accession code /H3K20260917 (https://github.com/HSPHSystemsSerology/H3K20260917).

Code Availability Statement

This manuscript utilizes the systems processor for integration of data for research (SPIDR), which is available for download through Zenodo (DOI: 10.5281/zenodo.20721204) (36). The analysis software uses an R-based programming language platform and can be run on any Windows-based operating system. The application was used for averaging technical replicates and subtraction of background signals.

Materials Availability Statement

All unique/stable reagents generated in this study are available from the lead contact with a completed materials transfer agreement and/or institutional licensing agreement.

Author Contributions

Conceptualization: Q.W., D.H.B., and R.P.M.

Methodology: Q.W., L.R.M., D.M., R.B., B.A.J., D.A.L., D.H.B., and R.P.M.

Software: Q.W. and R.P.M.

Validation: Q.W., D.M., B.A.J., D.A.L., A.Y.C., R.P.M.

Formal Analysis: Q.W., L.R.M., D.M., S.F., B.A.J., D.A.L., R.P.M.

Investigation: All authors

Resources: D.A.L., A.Y.C., D.H.B., and R.P.M.

Data Curation: Q.W., L.R.M., and D.M.

Writing: All authors

Visualization: Q.W., L.R.M., D.M., and R.P.M.

Supervision: Q.W., D.M., B.A.J., D.A.L., D.H.B., and R.P.M.

Project Administration: H.M.

Funding Acquisition. D.A.L., A.Y.C., D.H.B., and R.P.M.

Declarations of Generative AI and AI-Assisted Technologies

No artificial intelligence (AI) was used in the analysis of this study or in the writing of this manuscript.

References

1. Agor JK, Özaltın OY. Models for predicting the evolution of influenza to inform vaccine strain selection. Hum Vaccin Immunother. 2018;14(3):678–83. Epub 20180212. doi: 10.1080/21645515.2017.1423152. PubMed PMID: 29337643; PubMed Central PMCID: PMC5861780.
2. Maurer DP, Vu M, Schmidt AG. Antigenic drift expands influenza viral escape pathways from recalled humoral immunity. Immunity. 2025;58(3):716 – 27.e6. Epub 20250228. doi: 10.1016/j.immuni.2025.02.006. PubMed PMID: 40023162; PubMed Central PMCID: PMC11906258.
3. Sabaiduc S, Kaweski SE, Separovic L, Gao R, Ranadheera C, Bastien N, et al. Emergence of seasonal influenza A(H3N2) variants with immune escape potential warrants enhanced molecular and epidemiological surveillance for the 2025–2026 season. J Assoc Med Microbiol Infect Dis Can. 2025;10(4):281–98. Epub 20251031. doi: 10.3138/jammi-2025-0025. PubMed PMID: 42079493; PubMed Central PMCID: PMC13132565.
4. Lucaccioni H, Marques DF, Kirsebom F, Emborg HD, Hamilton M, Whitaker H, et al. Influenza vaccine effectiveness from nine studies during drifted A(H3N2) subclade K predominance, Europe, September 2025 to January 2026. Euro Surveill. 2026;31(7). doi: 10.2807/1560-7917.ES.2026.31.7.2600109. PubMed PMID: 41716088; PubMed Central PMCID: PMC12924001.
5. Wang L, Nangle SJ, Waller-Pulido A, McMahan K, Pereira J, Chaudhari J, et al. Vaccine-Elicited Antibody Responses to Influenza A(H3N2) Subclade K. JAMA. 2026. Epub 20260309. doi: 10.1001/jama.2026.2173. PubMed PMID: 41801760; PubMed Central PMCID: PMC12973212.
6. Waldock J, Weiss CD, Wang W, Levine MZ, Jefferson SN, Ho S, et al. An external quality assessment feasibility study; cross laboratory comparison of haemagglutination inhibition assay and microneutralization assay performance for seasonal influenza serology testing: A FLUCOP study. Front Immunol. 2023;14:1129765. Epub 20230228. doi: 10.3389/fimmu.2023.1129765. PubMed PMID: 36926342; PubMed Central PMCID: PMC10011125.
7. Wood JM, Major D, Heath A, Newman RW, Höschler K, Stephenson I, et al. Reproducibility of serology assays for pandemic influenza H1N1: collaborative study to evaluate a candidate WHO International Standard. Vaccine. 2012;30(2):210–7. Epub 20111117. doi: 10.1016/j.vaccine.2011.11.019. PubMed PMID: 22100887.
8. Truelove S, Zhu H, Lessler J, Riley S, Read JM, Wang S, et al. A comparison of hemagglutination inhibition and neutralization assays for characterizing immunity to seasonal influenza A. Influenza Other Respir Viruses. 2016;10(6):518–24. Epub 20160827. doi: 10.1111/irv.12408. PubMed PMID: 27406695; PubMed Central PMCID: PMC5059953.

9. Jacob-Dolan C, Hope D, Liu J, Waller-Pulido A, Verrette B, Cabrera-Barragan DN, et al. Adenovirus and mRNA vaccines as well as mucosal boosting improve protective efficacy against influenza virus challenge in macaques. Sci Transl Med. 2025;17(806):eadu7646. Epub 20250709. doi: 10.1126/scitranslmed.adu7646. PubMed PMID: 40632835.
10. Heeringa M, Leav B, Smolenov I, Palladino G, Isakov L, Matassa V. Comparability of Titers of Antibodies against Seasonal Influenza Virus Strains as Determined by Hemagglutination Inhibition and Microneutralization Assays. J Clin Microbiol. 2020;58(9). Epub 20200824. doi: 10.1128/JCM.00750-20. PubMed PMID: 32493784; PubMed Central PMCID: PMC7448638.
11. Wang Q, McManus LR, Levine KS, Blanc R, Malca H, Joughin BA, et al. A multiplexed, systems-based approach for prediction of antibody neutralization breadth for soluble human receptors. J Immunol. 2026;215(5). doi: 10.1093/jimmun/vkag106. PubMed PMID: 42179346; PubMed Central PMCID: PMC13200002.
12. Liu J, Li SH, Ye N, Griffiths T, Drapeau EM, Atkinson RK, et al. Antibodies Elicited by the 2025–2026 Influenza Vaccine. NEJM Evid. 2026;5(4):EVIDpha2600007. Epub 20260303. doi: 10.1056/EVIDpha2600007. PubMed PMID: 41774915.
13. Misyura M, Sukhai MA, Kulasignam V, Zhang T, Kamel-Reid S, Stockley TL. Improving validation methods for molecular diagnostics: application of Bland-Altman, Deming and simple linear regression analyses in assay comparison and evaluation for next-generation sequencing. J Clin Pathol. 2018;71(2):117–24. Epub 20170726. doi: 10.1136/jclinpath-2017-204520. PubMed PMID: 28747393; PubMed Central PMCID: PMC5800325.
14. Altman DG. Practical Statistics for Medical Research: Chapman and Hall/CRC; 1990. 624 p.
15. Dugan HL, Guthmiller JJ, Arevalo P, Huang M, Chen YQ, Neu KE, et al. Preexisting immunity shapes distinct antibody landscapes after influenza virus infection and vaccination in humans. Sci Transl Med. 2020;12(573). doi: 10.1126/scitranslmed.abd3601. PubMed PMID: 33298562; PubMed Central PMCID: PMC8115023.
16. Sevim Bayrak C, Forst CV, Jones DR, Gresham DJ, Pushalkar S, Wu S, et al. Patient subtyping analysis of baseline multi-omic data reveals distinct pre-immune states associated with antibody response to seasonal influenza vaccination. Clin Immunol. 2024;266:110333. Epub 20240730. doi: 10.1016/j.clim.2024.110333. PubMed PMID: 39089348; PubMed Central PMCID: PMC11340208.
17. Li SH, Wang B, Jo G, Mikelov A, Atkinson RK, Le Sage V, et al. Childhood immunological imprinting of cross-subtype antibodies targeting the hemagglutinin head domain of influenza viruses. Cell Host Microbe. 2026;34(5):873 – 87.e11. Epub 20260427. doi: 10.1016/j.chom.2026.04.004. PubMed PMID: 42049037.
18. Worobey M, Plotkin S, Hensley SE. Influenza Vaccines Delivered in Early Childhood Could Turn Antigenic Sin into Antigenic Blessings. Cold Spring Harb Perspect Med. 2020;10(10). Epub 20201001. doi: 10.1101/cshperspect.a038471. PubMed PMID: 31964642; PubMed Central PMCID: PMC7371515.

19. Liang CY, Raju S, Liu Z, Li Y, Asthagiri Arunkumar G, Case JB, et al. Imprinting of serum neutralizing antibodies by Wuhan-1 mRNA vaccines. Nature. 2024;630(8018):950–60. Epub 20240515. doi: 10.1038/s41586-024-07539-1. PubMed PMID: 38749479; PubMed Central PMCID: PMC11419699.
20. Plotkin SA, Gilbert PB. Nomenclature for immune correlates of protection after vaccination. Clin Infect Dis. 2012;54(11):1615–7. Epub 20120320. doi: 10.1093/cid/cis238. PubMed PMID: 22437237; PubMed Central PMCID: PMC3348952.
21. Offit SPWOP. Vaccines, 6th Edition: Saunders; 2012. 1570 p.
22. Skowronski DM, Chambers C, De Serres G, Sabaiduc S, Winter AL, Dickinson JA, et al. Vaccine Effectiveness Against Lineage-matched and -mismatched Influenza B Viruses Across 8 Seasons in Canada, 2010–2011 to 2017–2018. Clin Infect Dis. 2019;68(10):1754–7. doi: 10.1093/cid/ciy876. PubMed PMID: 30312364; PubMed Central PMCID: PMC6495010.
23. Erbelding EJ, Post DJ, Stemmy EJ, Roberts PC, Augustine AD, Ferguson S, et al. A Universal Influenza Vaccine: The Strategic Plan for the National Institute of Allergy and Infectious Diseases. J Infect Dis. 2018;218(3):347–54. doi: 10.1093/infdis/jiy103. PubMed PMID: 29506129; PubMed Central PMCID: PMC6279170.
24. Danesh A, Ren Y, Brad Jones R. Roles of fragment crystallizable-mediated effector functions in broadly neutralizing antibody activity against HIV. Curr Opin HIV AIDS. 2020;15(5):316–23. doi: 10.1097/COH.0000000000000644. PubMed PMID: 32732552; PubMed Central PMCID: PMC7748341.
25. Gunn BM, Lu R, Slein MD, Ilinykh PA, Huang K, Atyeo C, et al. A Fc engineering approach to define functional humoral correlates of immunity against Ebola virus. Immunity. 2021;54(4):815 – 28.e5. doi: 10.1016/j.immuni.2021.03.009. PubMed PMID: 33852832; PubMed Central PMCID: PMC8111768.
26. Bowman KA, Kaplonek P, McNamara RP. Understanding Fc function for rational vaccine design against pathogens. mBio. 2023:e0303623. Epub 20231219. doi: 10.1128/mbio.03036-23. PubMed PMID: 38112418.
27. Brown EP, Dowell KG, Boesch AW, Normandin E, Mahan AE, Chu T, et al. Multiplexed Fc array for evaluation of antigen-specific antibody effector profiles. J Immunol Methods. 2017;443:33–44. Epub 20170203. doi: 10.1016/j.jim.2017.01.010. PubMed PMID: 28163018; PubMed Central PMCID: PMC5333794.
28. Boesch AW, Brown EP, Cheng HD, Ofori MO, Normandin E, Nigrovic PA, et al. Highly parallel characterization of IgG Fc binding interactions. MAbs. 2014;6(4):915–27. doi: 10.4161/mabs.28808. PubMed PMID: 24927273; PubMed Central PMCID: PMC4171026.
29. Brown EP, Licht AF, Dugast AS, Choi I, Bailey-Kellogg C, Alter G, et al. High-throughput, multiplexed IgG subclassing of antigen-specific antibodies from clinical samples. J Immunol Methods. 2012;386(1–2):117 – 23. Epub 20120927. doi: 10.1016/j.jim.2012.09.007. PubMed PMID: 23023091; PubMed Central PMCID: PMC3475184.

30. Lasrado N, Wang L, Liu J, Rössler A, Chaudhari J, Wang Q, et al. An intramuscular prime and mucosal boost vaccine regimen protects against lethal clade 2.3.4.4b H5N1 challenge in cynomolgus macaques. Sci Transl Med. 2025;17(820):eady2282. Epub 20251015. doi: 10.1126/scitranslmed.ady2282. PubMed PMID: 41091914.
31. Bland JM, Altman DG. Statistical methods for assessing agreement between two methods of clinical measurement. Lancet. 1986;1(8476):307–10. PubMed PMID: 2868172.
32. Lin LI. A concordance correlation coefficient to evaluate reproducibility. Biometrics. 1989;45(1):255–68. PubMed PMID: 2720055.
33. Feyssaguet M, Bellanger A, Nozay F, Friel D, Merck E, Verlant V, et al. Comparison between a new multiplex electrochemiluminescence assay and the WHO reference enzyme-linked immunosorbent assay to measure serum antibodies against pneumococcal serotype-specific polysaccharides. Vaccine. 2019;37(16):2208–15. Epub 20190315. doi: 10.1016/j.vaccine.2019.03.011. PubMed PMID: 30879829.
34. Hartigan JA, Hartigan PM. The Dip Test of Unimodality. The Annals of Statistics1985. p. 70–84.
35. Wang J, Wen S, Symmans WF, Pusztai L, Coombes KR. The bimodality index: a criterion for discovering and ranking bimodal signatures from cancer gene expression profiling data. Cancer Inform. 2009;7:199–216. Epub 20090805. doi: 10.4137/cin.s2846. PubMed PMID: 19718451; PubMed Central PMCID: PMC2730180.
36. Wang Q, McNamara RP. Systems processor for integrated data for research (SPIDR) application. 1.0.1 ed2026.

Tables

Tables 1 and 2 are available in the Supplementary Files section.

Figures

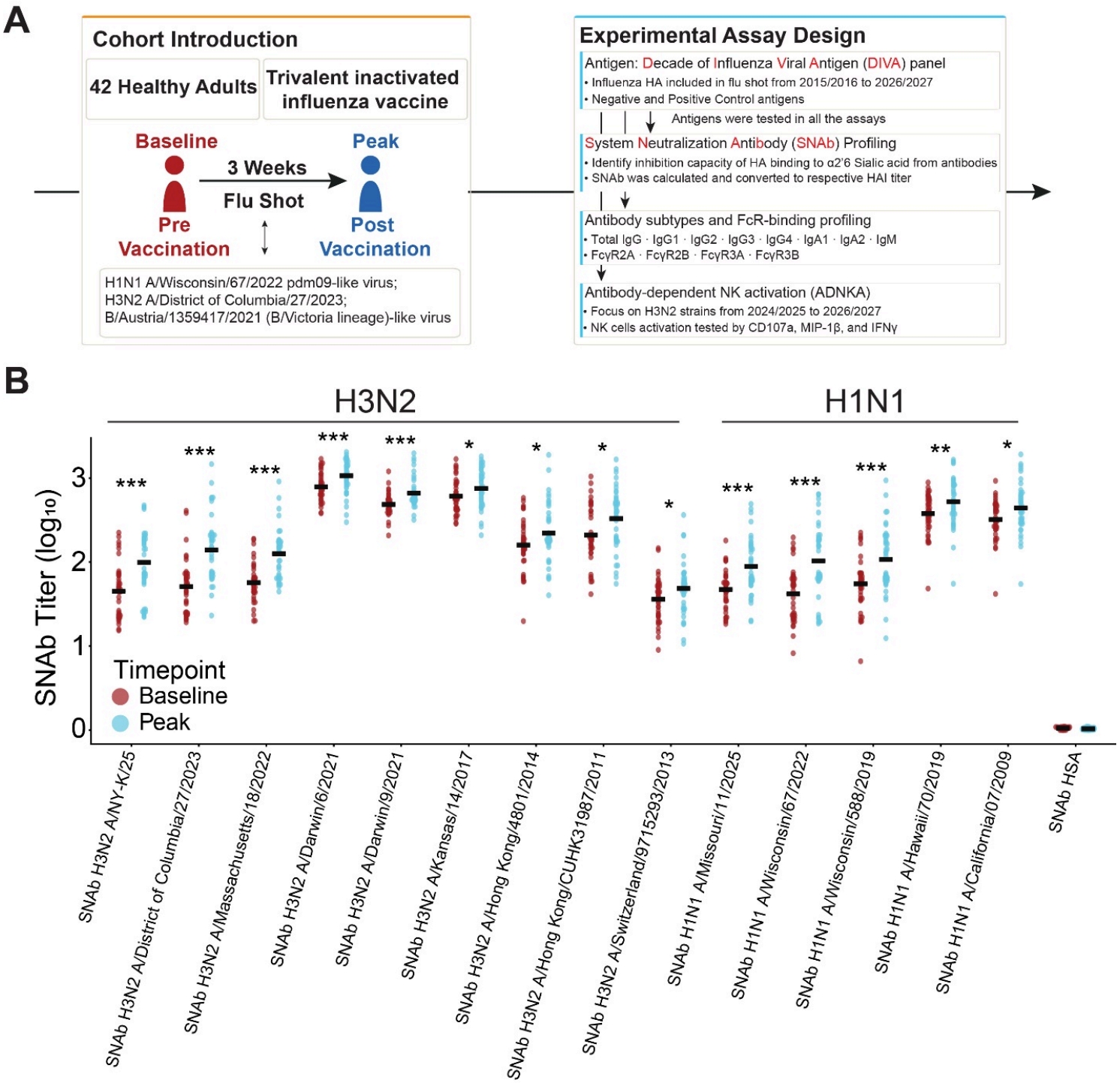


Figure 1

A decade-spanning antigen panel resolves predicted neutralization levels across the influenza vaccine strain history.

A. Cohort introduction and experimental design flowchart. A total of 42 healthy adults who received the 2025/2026 trivalent inactivated influenza vaccine H1N1 A/Wisconsin/67/2022 (H1N1)pdm09-like; H3N2 A/District of Columbia/27/2023; B/Austria/1359417/2021 (B/Victoria lineage)-like had serum collected before vaccination (baseline) and 3 weeks after vaccination (peak). The Decade of Influenza Virus

Antigen (DIVA) panel comprises hemagglutinin (HA) antigens from influenza A and B strains included in the seasonal vaccine from 2015/2016 to 2026/2027, together with positive and negative control antigens. All antigens were assayed in parallel by systems-predicted neutralizing antibody (SNAb) profiling, which quantifies antibody-mediated inhibition of HA binding to α2,6-linked sialic acid. Lastly, systems serology analysis through antibody isotype, subclass, and FcγR-binding profiling and antibody effector function assays were performed.

B. SNAb titers (log_{10}) against 14 vaccine-strain HA targets at baseline (red) and peak (blue) from the healthy adults. Horizontal bars indicate the median of titers. Human serum albumin (HSA) is shown as a non-specific binding control. Comparisons of pre- and post-vaccination titers for each target were done using a Wilcoxon Test followed by Benjamini–Hochberg correction: * = p < 0.05, ** = p < 0.01, *** = p < 0.001.

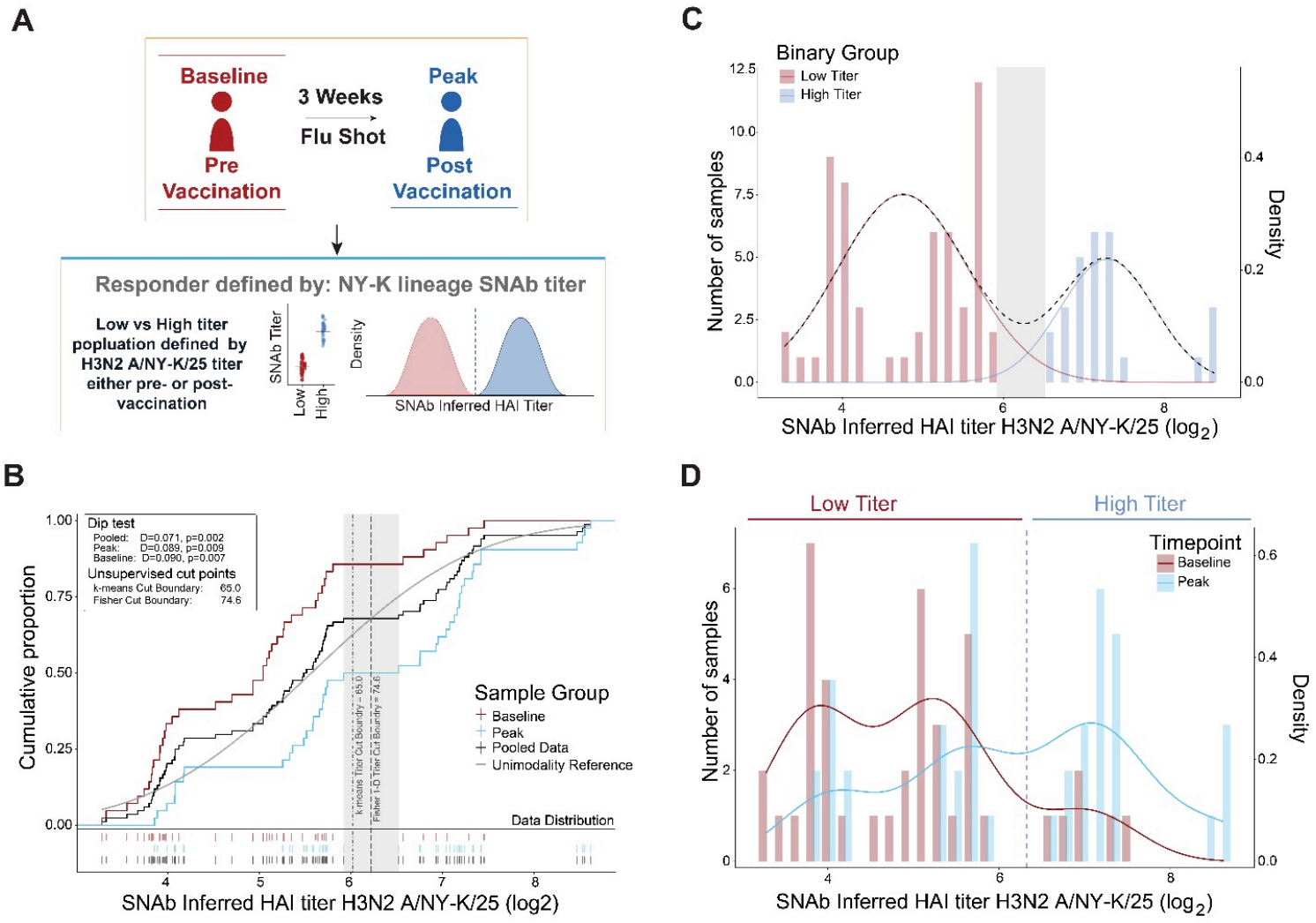


Figure 2

SNAb-inferred HAI titers against H3N2 subclade K separate subjects into two non-overlapping populations.

A. Schematic of the responder definition. Serum was collected at baseline and peak immune timepoints after receiving the 2025/2026 influenza vaccine. SNAb inferred HAI titers were quantified against the vaccine-mismatched H3N2 A/NY-K/25 at both collection times. Titers could then be modeled into a binary of low vs. high titers.

B. Empirical cumulative distribution of SNAb inferred HAI titers (log_2) for baseline (red), peak (blue), and pooled (black) samples, along with a unimodal reference distribution (grey). Hartigan's dip test rejected unimodality in the pooled data (D = 0.071, p = 0.002) and within each timepoint (peak D = 0.089, p = 0.009; baseline D = 0.090, p = 0.007). Cut points applied to the pooled data are marked (k-means 65.0; Fisher 74.6); shading marks the unpopulated interval. Rug marks below the axis show individual samples.

C. Distribution of the SNAb inferred HAI titers colored by assigned population. Curves are normal densities fitted to each population (low titer, red; high titer, blue), weighted by group size, with their sum shown in the dashed line. The grey area is the unpopulated cut point identified in B. On the x-axis is the SNAb inferred titer in log_2 units, and on the y-axis is the cumulative number of samples (left) and density of distribution (right).

D. The same distribution as **C**, but colored by collection time (red for pre-vaccination, and blue for post-vaccination).

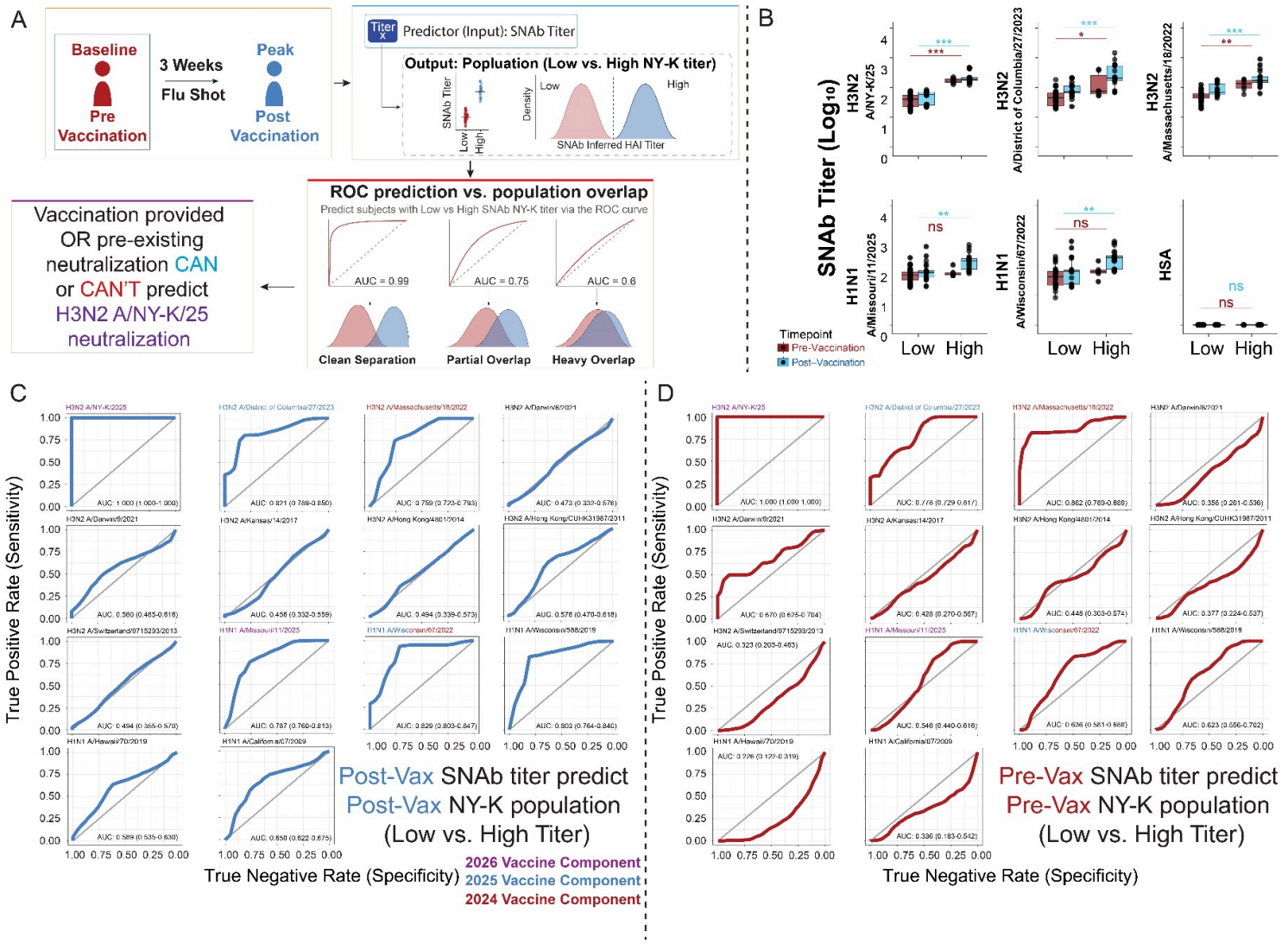


Figure 3

SNAb titers against recent H3N2 influenza vaccine components classify low and high titer phenotype to the 2025 mismatched subclade K.

A. Analysis workflow. The SNAb titer against a single influenza vaccine target is used as the predictor (input), and the low vs. high H3N2 A/NY-K/25 population as the outcome (output), which is evaluated for specificity and sensitivity by a receiver operating characteristic (ROC) curve. This is done for both pre- and post-vaccination collections.

B. SNAb titers (log_{10}) in the low- and high-titer classified H3N2 A/NY-K/25 populations for three most recent H3N2 vaccine targets (H3N2 A/NY-K/25 (control), A/District of Columbia/27/2023, and A/Massachusetts/18/2022; top row) and two recent H1N1 targets (A/Missouri/11/2025, A/Wisconsin/67/2022). HSA was used as a non-specific binding control. Pre-vaccination (red) and post-vaccination (blue) samples are shown separately. Comparisons by Wilcoxon test with Benjamini–Hochberg correction: * = p < 0.05, ** = p < 0.01, *** = p < 0.001; ns, not significant.

C. ROC curves using the post-vaccination SNAb titer against each indicated influenza vaccine target's ability to classify the post-vaccination low vs. high H3N2 A/NY-K/25 population. AUCs are given with bootstrap 95% confidence intervals; the diagonal indicates chance (AUC = 0.5). H3N2 A/NY-K/25 itself is used as an internal positive control. Strain labels are colored to mark the targets reaching validated discrimination ($p < 0.05$ for model accuracy) and for the year that the influenza virus target was included in the annual vaccination; purple = 2026, blue = 2025, and red = 2024. H1N1 HA A/Wisconsin/67/2022 is colored in blue and red as it was included in the 2024 and 2025 influenza vaccine formulation.

D. Same as in **C**, but using the pre-vaccination SNAb titer against each indicated influenza vaccine target's ability to classify the pre-vaccination low vs. high H3N2 A/NY-K/25 (NY-K lineage) population.

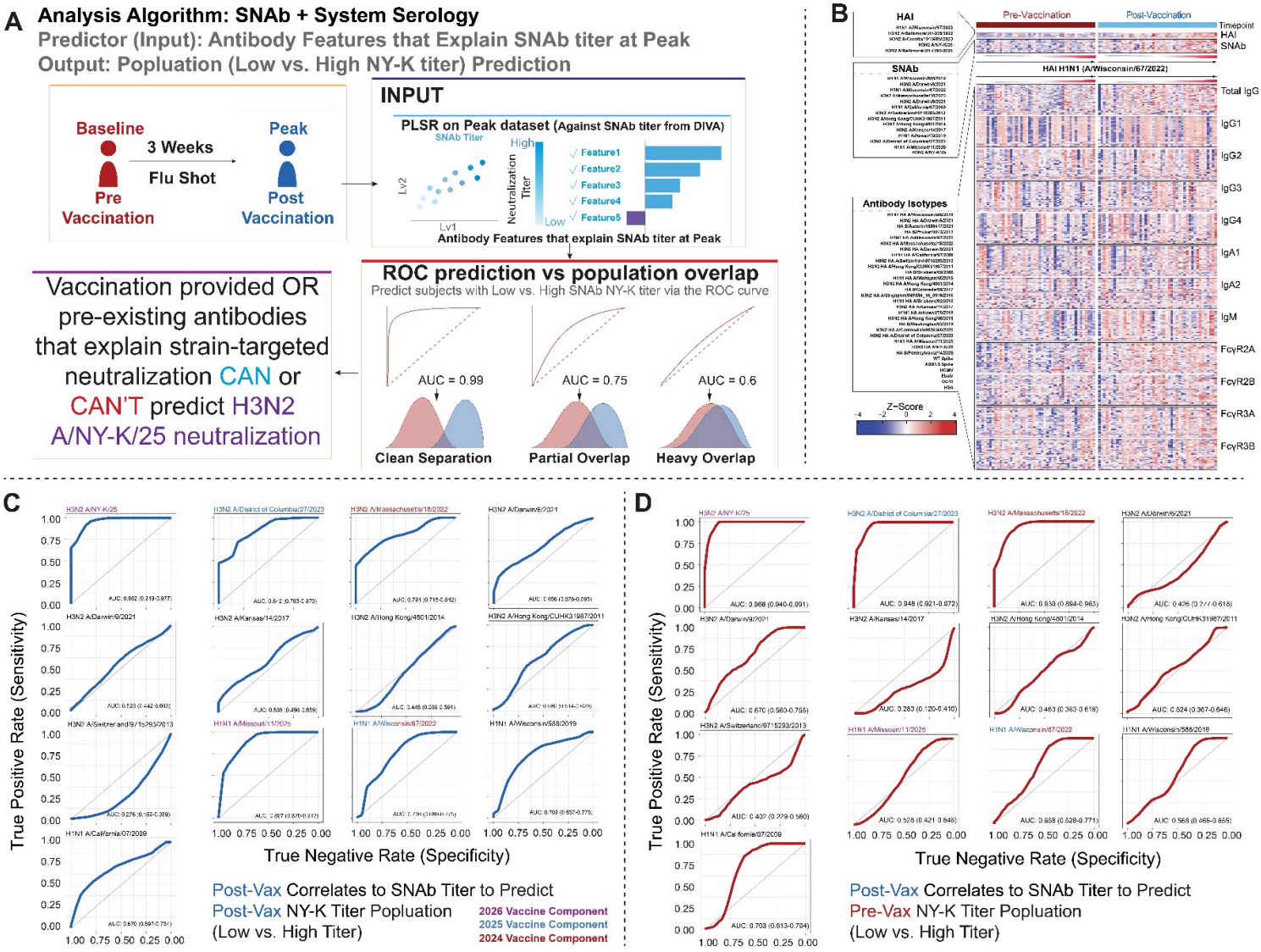


Figure 4

Systems serology features against recent H3N2 influenza vaccine components classify low and high titer phenotypes to the 2025 mismatched subclade K.

A. Analysis workflow. Comprehensive antibody isotype, subclass, and Fc-receptor binding features measured post-vaccination are modelled by PLSR against each SNAb titer from the DIVA panel. The least absolute shrinkage and selection operator (LASSO) identified features that explain the SNAb titer are carried forward as the predictor (input), and the low vs high H3N2 A/NY-K/25 (NY-K lineage) population as the outcome (output), which is evaluated for specificity and sensitivity by ROC.

B. Heatmap of the neutralization and antibody-feature landscape across the DIVA panel. Rows are grouped by measurement class: HAI and SNAb titers (top), followed by total IgG, IgG1–IgG4, IgA1, IgA2, IgM, and binding to FcγR2A, FcγR2B, FcγR3A, and FcγR3B. Columns are individual samples, separated by timepoint (pre- and post-vaccination) and ordered within each timepoint by HAI titer against H1N1 A/Wisconsin/67/2022 previously reported (5). Values are $\log_{10}$-transformed z-scores computed across all samples. Antigen identities for each block are listed at left.

C. ROC curves using the post-vaccination LASSO-identified antibody signature that correlates with the SNAb titer of each indicated strain to classify the post-vaccination low vs. high H3N2 A/NY-K/25 (NY-K lineage) population. AUCs are given with bootstrap 95% confidence intervals; the diagonal indicates chance. The H3N2 A/NY-K/25 LASSO-identified antibody signature to predict itself serves as an internal positive control. Strain labels are colored to mark the targets reaching validated discrimination ($p < 0.05$ for model accuracy) and the year that the influenza virus target was included in the annual vaccination; purple = 2026, blue = 2025, and red = 2024. H1N1 A/Wisconsin/67/2022 is colored in blue and red as it was included in the 2024 and 2025 influenza vaccine formulation. No LASSO-based model could be built for H1N1 A/Hawaii/2019, thus no classification test was done for this strain.

D. Same as in **C**, but using the same post-vaccination-derived signatures to classify the pre-vaccination low vs. high H3N2 A/NY-K/25 (NY-K lineage) population.

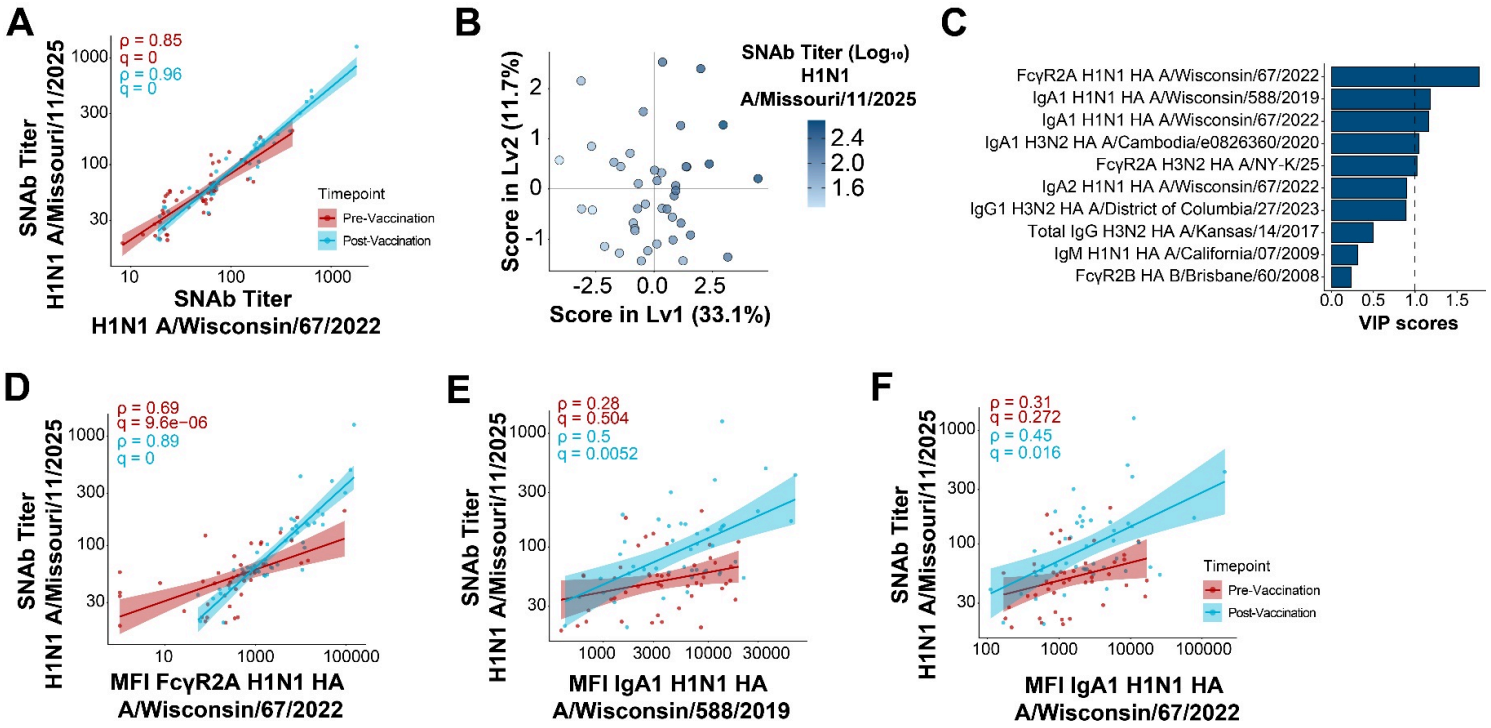


Figure 5

Vaccination-induced neutralization levels and antibody features against the 2025 target strain H1N1 A/Wisconsin/67/2022 provide a foundation for the 2026 vaccine target H1N1 A/Missouri/11/2025.

A. Correlation between SNAb titers against H1N1 A/Wisconsin/67/2022 and H1N1 A/Missouri/11/2025 at either pre-vaccination (red) or post-vaccination (blue). Lines are fitted with 95% confidence bands; ρ = Spearman's rho; q = Bonferroni-adjusted p value. A q value of 0 indicates machine zero.

B. Partial least-squares regression (PLSR) scores for the model relating LASSO-selected antibody features to SNAb titer against H1N1 A/Missouri/11/2025 at peak. Each point is one subject, shaded by SNAb titer (log_{10}). Axes give the percentage of variance captured by latent variable 1 (LV1) (33.1%) and LV2 (11.7%).

C. Variable importance in projection (VIP) scores for the LASSO-selected features. The dashed line marks VIP = 1; features exceeding this threshold were taken as the major contributors to the model separation (see Methods). The top three features were carried forward to confirmatory analysis.

D. Univariate correlations between the SNAb titer against H1N1 A/Missouri/11/2025 and the VIP feature in **C.**, FcγR2A H1N1 HA A/Wisconsin/67/2022. Shown are values for pre- and post-vaccination collections. Lines are fitted with 95% confidence bands; ρ = Spearman's rho; q = Bonferroni-adjusted p value. A q value of 0 indicates machine zero.

E. Univariate correlations between the SNAb titer against H1N1 A/Missouri/11/2025 and the VIP feature in **C.**, IgA1 H1N1 HA A/Wisconsin/588/2019. Shown are values for pre- and post-vaccination collections. Lines are fitted with 95% confidence bands; ρ = Spearman's rho; q = Bonferroni-adjusted p value. A q value of 0 indicates machine zero.

F. Univariate correlations between the SNAb titer against H1N1 A/Missouri/11/2025 and the VIP feature in **C.**, IgA1 H1N1 HA A/Wisconsin/67/2022. Shown are values for pre- and post-vaccination collections. Lines are fitted with 95% confidence bands; ρ = Spearman's rho; q = Bonferroni-adjusted p value. A q value of 0 indicates machine zero.

Supplementary Files

This is a list of supplementary files associated with this preprint. Click to download.

- SupplementaryInformationVaccineMismatch20261007.docx
- Tables27.docx